J Solid State Electrochem (2012) 16:1255–1262
DOI 10.1007/s10008-011-1522-5

ORIGINAL PAPER

Potentiostatic versus galvanostatic electrodeposition of nanocrystalline Al–Mg alloy powders

Sankara Sarma V. Tatiparti · Fereshteh Ebrahimi

Received: 13 May 2011 / Revised: 29 June 2011 / Accepted: 2 August 2011 / Published online: 17 August 2011

Abstract Nanocrystalline supersaturated dendritic Al–Mg powders were electrodeposited using potentiostatic and galvanostatic techniques under equal-charge conditions. In potentiostatic deposition morphology depended on applied potential: featherlike at lower and globular at higher potentials. Galvanostatic deposits yielded both morphologies at any current density. Morphological evolution was observed in galvanostatic deposits from featherlike to globular. Independent of deposition technique face-centered cubic Al(+Mg) phase with ~7 atom% Mg (featherlike) with/without ~20 atom%Mg (smooth globular) composition formed at lower applied/realized potentials (or deposition rates). Higher applied/realized potentials showed hexagonal close packed Mg(+Al) phase with ~80 atom% Mg (rough globules) over smooth globules. Potentiostatic and galvanostatic deposits were compared for their morphologies, phases, and compositions.

Keywords Al · Mg · Electrodeposition · Potentiostatic · Galvanostatic

S. S. V. Tatiparti (✉) · F. Ebrahimi
Materials Science and Engineering Department,
University of Florida,
Gainesville, FL 32611, USA
e-mail: sankara@ufl.edu

Present Address:
S. S. V. Tatiparti
General Motors Technical Center India Pvt. Ltd,
3rd Floor, Creator Building, ITPL,
Bangalore, India 560 066
e-mail: sankarasarma.tatiparti@gm.com

Introduction

Electrodeposition is a versatile technique offering several parameters such as current density (overpotential), electrolyte composition, pH, substrate material, etc. to produce powders with various characteristics. Electrodeposition of powders can be conducted using either potentiostatic or galvanostatic technique. Using galvanostatic deposition technique powders with several characteristics can be obtained in a single deposit. For example, using this technique at low-applied current densities, Cu particles with both massive dendritic structure and 3D ramified structure were obtained within the same deposit [1]. When the current density was increased the massive dendritic structure disappeared rendering only 3D ramified structure. Moreover, the particle size decreased with current density indicating the influence of deposition rate. Galvanostatic deposition can be useful in applications where no control over morphology is necessary.

Potentiostatic deposition technique, on the other hand, was mainly used to investigate the mechanism of deposit morphology formation [2, 3]. For example, at lower deposition potentials, anisotropic branched dendrites were obtained in Cu electrodeposition [2]. The extent of branching of these dendrites was increased at higher deposition potentials. However, unlike in the galvanostatic deposition, the morphology was specific to the applied potentials (E). It was shown in literature that the formation of a morphology requires a critical energy for nucleation [4] which is supplied by the applied potential in potentiostatic deposition. Hence, by controlling the applied potential deposits with uniform and desired morphologies can be obtained using potentiostatic deposition. Thus, potentiostatic deposition technique can find significant use in applications

where morphology control is critical, e.g., optical and electrical applications requiring specific crystallographic planes [5].

The use of appropriate technique is essential to produce materials with desired properties. This necessitates understanding the contrast between potentiostatic and galvanostatic deposition to use them effectively for powder production. Vast literature is available on powder production with either technique. However, there are only few reports on direct comparison of these two techniques applied on either single metal or thin film deposits [4, 6, 7]. Comparative study on these two techniques in the context of alloy powder deposition has not received much attention. Alloy systems are a little complicated to study because not only morphologies but also different phases and their compositions could change with deposition technique.

We were successful in producing nanocrystalline, supersaturated dendritic Al–Mg alloy powders for H_2-storage application using galvanostatic deposition technique [8]. Our detailed morphological and microstructural analyses showed that nanocrystalline Al–Mg dendrites appeared with featherlike and globular morphologies [9]. In the present study, we conducted electrodeposition of Al–Mg alloy powders using both potentiostatic and galvanostatic deposition techniques under equal charge conditions. The morphologies, phases, and compositions of the deposits from these two techniques were explained on the basis of the differences between potentiostaic and galvanostatic deposition techniques.

Experimental

Al–Mg alloys were electrodeposited using an organometallic-based electrolyte with composition 1 M $Na[AlEt_4]$+2 M $Na[Et_3Al\text{-}H\text{-}AlEt_3]$+2.5 M $AlEt_3$+6 M toluene in a glove box. The details of the electrolyte preparation were reported elsewhere [8]. A rotating cylinder cell setup consisting of Cu rod of diameter 6 mm as cathode rotating at 200 rpm and an annular Mg anode was used for deposition. The Cu cathode was electropolished outside the glove box using an electrolyte made of 82.5 vol.% ortho-H_3PO_4 and 17.5 vol.% deionized (DI) water. The polished rod was rinsed with DI water and dried prior to transferring into the glove box. Mg was introduced into the electrolyte by a process which we termed pre-electrodeposition [10]. The duration of the pre-electrodeposition (90 min) was kept constant for all the experiments such that a saturated amount of Mg enters into the electrolyte. A PAR 273 potentiostat/galvanostat interfaced with a computer was used for the deposition experiments.

Electrodeposition experiments were conducted at 60 °C and up to 15 min (900 s) using a freshly prepared polycrystalline copper electrode for each deposition. The Al–Mg alloy powders were produced using both potentiostatic and galvanostatic techniques. The potentiostatic depositions were conducted at applied potentials E=−4 and −5 V. For galvanostatic experiments, the initial current density values were chosen based on those obtained during potentiostatic experiments. Apparent current densities of j= 30 and 60 mA cm^{-2} based on the initial surface area of the Cu cathode were employed in galvanostatic experiments. These current densities were around or above the limiting diffusion current density value, j_L=38 mA cm^{-2} rendering deposit growth in mass transfer regime [3]. A non-aqueous Ag/AgCl reference electrode filled with 1 M LiCl in ethylene glycol monobutyl ether was used for controlling (potentiostatic) or monitoring (galvanostatic) the potentials.

The deposits were cleaned while on the cathode three times by rotating it in toluene for about 10 min. The cleaned powders were characterized using APD XRD 3720 powder diffractometer with Cu K_α radiation for phase identification. The morphologies were characterized using a JEOL 6400 scanning electron microscope (SEM). The composition of these powders was analyzed using the wavelength dispersive spectroscopy technique in an electron probe micro-analyzer (EPMA) JEOL 733. The EPMA analysis was conducted on samples prepared by metallographic techniques.

Results

SEM images of the potentiostatic deposits at E=−4 and −5 V are shown in Fig. 1a and b, respectively. When E=−4 V, the Cu cathode was uniformly covered with several small nuclei some of which grew further and assumed featherlike morphology (marked as “A” in Fig. 1a). However, the size of this morphology varied from those in their early stages of growth (appear as small dots in Fig. 1a) to the significantly grown ones. The appearance of featherlike morphology over the entire area of the cathode indicates the almost uniform nature of the potentiostatic deposition process. When the applied potential was increased to E=−5 V deposit with only globular morphology appeared as shown in Fig. 1b. The globular morphology suggests the isotropic growth nature of this morphology. The globules form in two roughness levels: the rough ones (marked as “C”) always forming over the smooth ones (marked as “B”). The globular morphology appeared across the whole deposit with almost full coverage on the Cu cathode. All the morphologies observed here are nanocrystalline in nature [3]. An important observation from the deposits made using potentiostatic technique is that the obtained morphology was specific to the applied potential.

The galvanostatic deposits presented a different scenario than their potentiostatic counterparts. The SEM images of the galvanostatic deposits are presented in Fig. 2. Approximately,

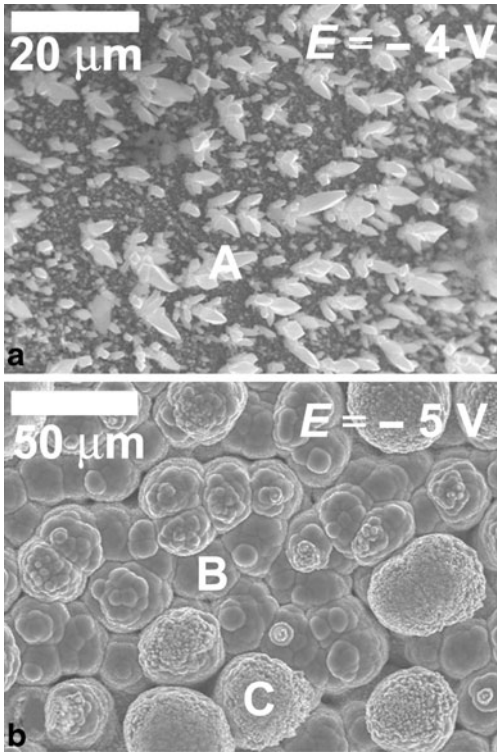

Fig. 1 SEM images of deposits made at **a** E=−4 V showing featherlike morphology (A) and **b** E=−5 V showing globular morphology with smooth (B) and rough (C) globules

the average values of the current densities realized in potentiostatic depositions (~30 mA cm^{-2} at E=−4 V and ~60 mA cm^{-2} at E=−5 V) were chosen as the initial nominal applied current densities in galvanostatic depositions. In this way, the deposition rates (in terms of current densities) and the total apparent charge density of the deposits was kept approximately the same in deposits at j=30 mA cm^{-2} and E=−4 V (~505 mC cm^{-2}) and j=60 mA cm^{-2} at E=−5 V (~1,090 mC cm^{-2}) separately. This enabled a direct comparison between potentiostatic and galvanostatic counterparts. The deposit at j=30 mA cm^{-2} shows both the featherlike and the smooth globular morphologies (marked as "A" and "B", respectively) of which the former is in majority (Fig. 2a). A low magnification image of the same deposit is shown in Fig. 2b and indicates vast areas where no deposit was formed on the Cu cathode. For a given initial nominal cathode area, approximately the same amount of charge as that of deposit at E=−4 V was deposited (equal apparent charge density). However, in the deposit at j= 30 mA cm^{-2}, since this charge was accommodated in much smaller area than its potentiostatic counterpart, this deposit grew to a much larger extent. The deposit made at j= 60 mA cm^{-2} also showed both featherlike and globular morphologies (marked as "A" and "B", respectively). However, here the globular morphology is in majority (Fig. 2c). The average length of the dendrites is ~250 μm

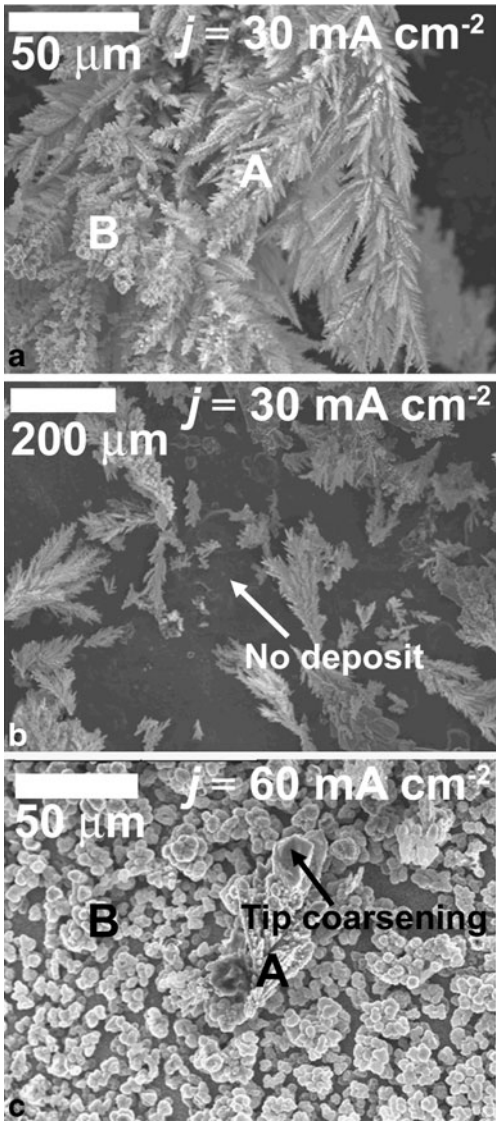

Fig. 2 SEM images of deposits made at **a** j=30 mA cm^{-2}, **b** j= 30 mA cm^{-2} (low magnification, region where no deposit formed is indicated by *arrow*), and **c** j=60 mA cm^{-2} showing featherlike (A) and globular (B) morphologies

in this case. Interestingly, the featherlike morphology in the deposit at j=60 mA cm^{-2} starts to coarsen at their tips as shown in Fig. 2c. A closer view of a well-defined featherlike morphology with coarse tips is shown in Fig. 3 and indicates its evolution into large smooth globules and eventually to rough globules. Similar observations were found in the electrodeposition of Co powders [11] and Ag–Au alloys [12] where disperse growing entities eventually coarsened at their tips and evolved into compact entities. Formation of the spherical diffusion zones was mentioned to be the reason for the realization of compact growth at later stages. The deposits made using galvanostatic technique yielded both featherlike and globular morphologies unlike their potentiostatic counterparts where the applied potential governed the type of morphology appeared.

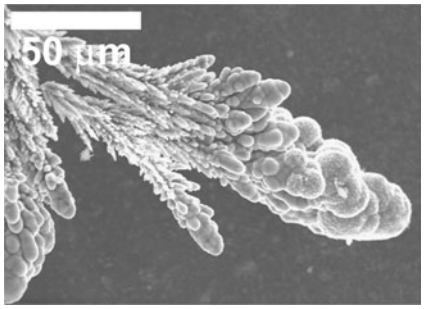

Fig. 3 SEM image showing morphological evolution from featherlike to globular morphology

The recorded values of apparent current density (in potentiostatic depositions) and E (in galvanostatic depositions) are plotted in Fig. 4 versus time. In the initial stage of the potentiostatic deposition, the apparent current density increased rapidly for both the applied potentials as shown in Fig. 4b. This rapid increase in the current density indicates the double-layer charging during which cations assemble in front of the cathode [13]. Following the double-layer charging, the current density dropped in both the applied potentials. The drop in the current density can be expected when the initial nuclei form in the beginning of the deposition, consuming the majority of the ions accumulated in front of the cathode. These nuclei can be seen in the SEM image of the deposit made at E=−4 V (Fig. 1a) whereas no such nuclei can be seen in deposit at E=−5 V (Fig. 1b) due to extensive formation of globular morphology. When the applied potential was −4 V, the current density decreased at a slower rate than at −5 V (Fig. 4b) suggesting a lower deposition rate and fewer nuclei at −4 V. The current density increased with time after the nucleation events for both the potentials due to the enhanced roughness of the deposits caused by the growth of the deposits. Consistently, the increase in the current density was more pronounced at the higher deposition potential (E=−5 V). The varying potential values as function of time during the galvanostatic deposition are shown in Fig. 4c, which shows that initially the potentials were very negative and then became less negative with time before reaching almost a saturation value for both the current densities j=30 and 60 mA cm^{-2}. The initial potential is governed by the nucleation of the Al–Mg alloy crystals on the cathode surface. Although the applied current density was kept constant, the real current density is expected to decrease during deposition due to the increasing surface area of the deposition front. The potential and the current density are related in semi-logarithmic fashion as $E \alpha \log(j)$ [14]. Hence, the decrease in the real current density is partially responsible for the reduction of the observed potential (Fig. 4c). The fact that the observed or the applied apparent current density values are around or above the limiting diffusion current density value (j_L=38 mA cm^{-2} [3]) and the dendritic morphology of the deposits suggest that the

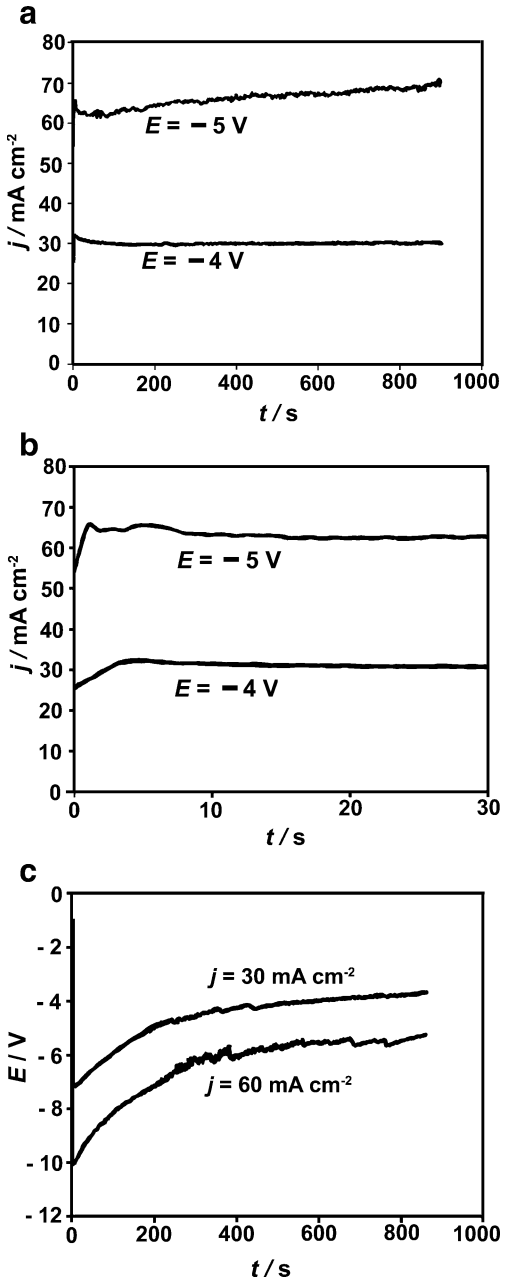

Fig. 4 **a** j–t curves of potentiostatic deposits at E=−4, −5 V up to 900 s, **b** j–t curves of potentiostatic deposits at E=−4, −5 V up to 30 s, **c** E–t curves of galvanostatic deposits at j=30 and 60 mA cm^{-2} up to 900 s

depositions were done at mass transfer regime. An estimation of the diffusion layer thickness can be obtained for the present rotating cylinder cell setup using Eq. 1 [15]:

$$\delta = 12.64 d^{0.3} \nu^{0.344} D_M^{0.356} V^{-0.7} \quad (1)$$

Where δ is the global diffusion layer thickness, d is the electrode diameter (6 mm), ν is the kinematic viscosity of electrolyte (for organometallic solutions, 0.003928 m^2 s [16]), D_M is the diffusion coefficient of ions (1.5 10^{-10} m^{2}s^{-1}

[17]), and V is the peripheral velocity ($\pi d\omega$) where ω: electrode angular velocity (20.9 rad s^{-1}). The estimated value of the diffusion layer thickness is 328 μm which is larger than the average length of the dendrites (~250 μm).

The phase and compositional analyses on the deposits are presented in Figs. 5 and 6, respectively. When the deposition rates (i.e., either recorded or applied apparent current densities) were lower for example in the case of deposits at E=−4 V and j=30 mA cm^{-2} only face-centered cubic (fcc) solid solution was observed (Fig. 5). At higher deposition rates, i.e., at E=−5 V and j=60 mA cm^{-2}, both fcc and hexagonal close packed (hcp) solid solutions formed (Fig. 5). Since E α log(j), the deposition rates (or current densities) are directly proportional to the applied (in potentiostatic) or the realized (in galvanostatic) potentials. The EPMA compositional analyses on the featherlike and globular morphologies are shown in Fig. 6a and b, respectively. The morphologies from both potentiostatic and galvanostatic techniques showed similar composition values. The featherlike morphology showed average composition of ~7 atom%Mg (Fig. 6a). Interestingly in the globular morphology, up to a large extent of the length of dendrites, which was spanned by the smooth globules, the composition remained almost constant at ~20 atom%Mg. Beyond this, in the region where rough globules were formed, the composition showed a sudden jump in the values to ~80 atom%Mg. The boundary where a sudden composition change was observed was indicated with a dashed line in Fig. 6b. Such a sudden and large jump is normally associated with the formation of the Mg-rich phase. Detailed compositional, phase analysis confirmed

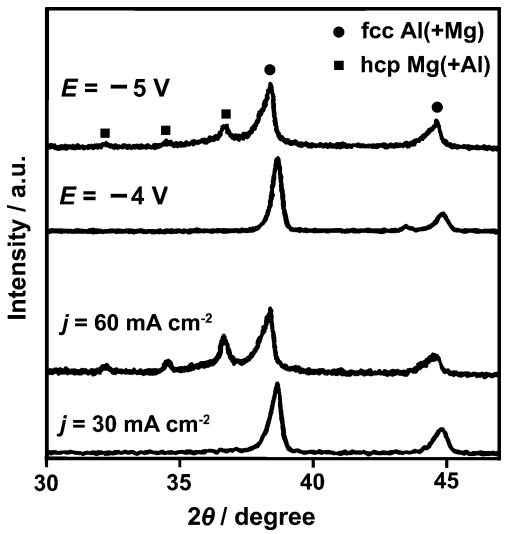

Fig. 5 XRD patterns of deposits made using potentiostatic and galvanostatic techniques showing fcc Al(+Mg) (circle) and hcp Mg(+Al) phases (*square*)

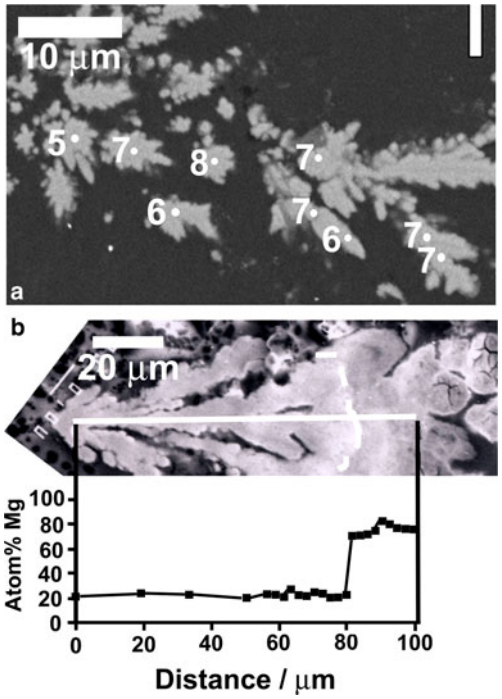

Fig. 6 EPMA results showing the compositional variation (atom% Mg) in dendrites with **a** featherlike and **b** globular morphology

that the smooth globules are made of fcc Al(+Mg) solid solution and rough globules possess hcp Mg(+Al) solid solution [3]. According to the equilibrium phase diagram, Al and Mg showed a mutual solubility of less than 1 atom% [18]. At higher compositions, two intermetallics namely Al_3Mg_2 and $Al_{12}Mg_{17}$ are found in Al–Mg system. The absence of any intermetallics in the present deposits at such high-composition values suggests that the deposition rates are so high that the deposition took place in non-equilibrium manner resulting in supersaturated and metastable phases [8]. The phase and composition results indicate that irrespective of the deposition technique, the deposits made at similar deposition rates, or applied/realized potentials possessed the same phases.

Discussion

The presented results suggest that morphology is specific to deposition technique. For example, in potentiostatic deposition featherlike morphology forms at E=−4 V and globular morphology appears at E=−5 V. In galvanostatic deposition, both the morphologies appeared in any deposit. For the present deposition conditions, the phases and compositions of the deposits were found to be morphology specific and dependent on deposition rate or the applied/realized potentials. At lower applied/realized potentials (at E=−4 V and j=30 mA cm^{-2}) fcc Al(+Mg) phase formed

with compositions of ~7 atom%Mg (featherlike) and ~20 atom%Mg (smooth globular). The higher applied/realized potentials resulted in hcp Mg(+Al) phase (with 80 atom%Mg in the form of rough globules) over the fcc Al(+Mg) phase. The results of the present study can be explained using the contrast in the deposit formation between potentiostatic and galvanostatic techniques.

In potentiostatic deposition where the applied potential is kept constant, the ions are released to cathode to maintain its surface at desired potential. Since the potential value is same everywhere on the surface of the cathode irrespective of the surface roughness, the spatial distribution of the concentration of Al^{+3} and Mg^{+2} ions along the surface of the cathode remains uniform. A critical potential is needed for formation of any morphology [4]. For example, a critical potential was identified to trigger the formation of single crystalline Zn dendrites via electrodeposition [19]. If the cathode surface potential is above the critical value needed for formation of a particular morphology, then that particular morphology nucleates and grows everywhere on the surface, e.g., featherlike morphology at $E=-4$ V (Fig. 1a) and globular morphology at $E=-5$ V (Fig. 1b). Our earlier work showed that the featherlike morphology always forms at $E=-4$ V (in magnitude) and the globular morphology is realized at potentials $E>-4$ V (in magnitude) [3]. At $E=-4$ V due to the lower recorded current density value (30 mA cm^{-2} in Fig. 4a), the depositing ions have enough time for arranging themselves in low-energy configurations resulting in featherlike morphology. Interestingly, our recent detailed crystallographic analysis reported elsewhere showed that the featherlike morphology grows with its stem and several higher-order arms oriented in specific crystallographic directions rendering not only morphological but also crystallographic anisotropy to this morphology [9]. At higher applied potential of $E=-5$ V since the recorded current density value is higher (60 mA cm^{-2} in Fig. 4a), the depositing ions do not have enough time for settling in low-energy configurations. Hence, the growth assumes isotropic nature with spherical-looking globular morphology (Fig. 1b). The appearance of different morphologies at different applied potentials indicates that the potential plays an important role in deciding the morphology of the deposits.

The galvanostatic deposition poses different requirements. Here, the current or the apparent current density (based on the initial surface area of the cathode) remains constant. Hence, the ions are released to cathode only to maintain constant apparent current density. No control is exercised over the potential on the cathode surface. So the ions released towards the cathode could distribute themselves in a random fashion. This random arrangement of ions over the cathode stems partially from the surface roughness. Systematic investigations on Cu electrodeposition showed that the growth occurs at a faster rate on the more elevated points of the cathode than at the average height of it [14]. The faster rates of deposition result in higher local potentials at these elevated points. This way, the resulting local potential values can be different at different locations on the cathode surface in galvanostatic deposition. These local potentials are extremely difficult to measure. If the locally realized potential satisfies the energy requirements for formation of a particular morphology, then that morphology nucleates and grows on that particular position on the cathode. In the deposit at lower apparent current density (30 mA cm^{-2}), there were vast areas on the substrate where no deposit was found (Fig. 2b). This suggests that the local potentials were not favorable for formation of any deposit in these areas. Also, there were relatively many spots on the cathode where the local potentials were favorable for formation of featherlike morphology. However, there were very few spots where the smooth globular morphology appeared (Fig. 2a) suggesting the presence of higher local potentials at these spots. This observation is consistent with the fact that featherlike morphology requires lower energy for nucleation whereas globular morphology requires higher energy for nucleation [3]. At higher apparent current density of 60 mA cm^{-2}, the trend in the appearance of majority morphology reversed. In this case, there were many spots where globular morphology appeared as majority due to possible higher local potentials in those spots. Moreover, at higher deposition rates, eventually rough globules which possess hcp Mg(+Al) phase appeared (Fig. 5 and 6b). With the random deposit growth in galvanostatic deposition, the surface area increases drastically which is reflected in the decreased overall potential values with time as shown in Fig. 4c.

The morphological evolution in the galvanostatic deposition is very interesting and only observed at higher current density (60 mA cm^{-2}; Fig. 3). The initially featherlike morphology eventually coarsened and evolved into smooth globules over which rough globules nucleated. Coarsening basically means that the tips of the featherlike morphology experienced a higher concentration of locally accumulated ions which deposited at higher rates resulting in globular morphology formation. Although, during the galvanostatic deposition, the overall current densities decrease due to the increased surface area of the deposits, the local current density values could be very high, e.g., on the tips of the featherlike morphology which possess very small surface area [14]. Similar to local potentials, these local current densities are very difficult to measure. However, an estimate for the current density around the tips of the featherlike morphology can be obtained. The tips of the featherlike morphology

experience current densities both at their tips and sides according to Eqs. 2 and 3, respectively [14]:

$$j_{L,tip} = j_L\left[1 + \frac{h}{r}\right] \quad (2)$$

$$j_{L,side} = j_L\frac{\delta}{\delta - h} \quad (3)$$

where, h is the height of the dendrites (250 μm) and r is the tip radius of featherlike morphology (1.2 μm). The estimated current densities at tip and its sides of the featherlike morphology are 7,536 and 160 mA cm^{-2}, respectively, and their sum is much larger than j_L. At such high current densities, the ions can distribute around the tips of the featherlike morphology leading to realization of spherical diffusion zones [20] resulting in tip coarsening and eventual formation of globular morphology. The results of the galvanostatic deposition suggest that the spatial and temporal variations in the local potentials caused by different deposition rates on the cathode surface and with the progress of dendritic growth respectively can result in the formation of the different morphologies.

The formation of a phase is essentially a nucleation event which requires a critical amount of energy. In the present case, this critical energy is supplied through either applied (potentiostatic) or realized (galvanostatic) potential. Irrespective of the deposition technique or the applied/realized potentials, always fcc Al(+Mg) phase nucleated on the surface of the cathode (Fig. 5). This indicates that for present experimental conditions only fcc Al(+Mg) meets the energy requirements and thus nucleates on the cathode. We have shown earlier that the amount of Mg in the deposits increases with current density or potential and the duration of deposition [8, 10]. Hence, the featherlike morphology formed at lower applied (E=−4 V) or locally realized (majority in j= 30 mA cm^{-2} and minority in j=60 mA cm^{-2}) potentials contained only ~7 atom%Mg. Similarly, the globular morphology deposited on the cathode at higher applied (E=−5 V) or locally realized (majority in j=60 mA cm^{-2} and minority in j=30 mA cm^{-2}) potentials possessed ~20 atom%Mg (Fig. 6). With further deposition following the formation of fcc Al(+Mg) phase on the cathode the electrolyte was enriched with Mg [10] and encouraged the formation of hcp Mg(+Al) phase with composition ~80 atom%Mg in the deposits done at E=−5 V or j= 60 mA cm^{-2} (Figs. 5 and 6b). The hcp Mg(+Al) phase could never nucleate right on the cathode. We have shown recently that the formation of hcp Mg(+Al) phase on the cathode surface was only successful when we employed hcp Mg substrate as cathode [21]. Lower critical nucleation energy estimated for formation of stable hcp Mg (+Al) nuclei on the Mg cathode was attributed as the reason for this observation. The observations on different phases and their compositions suggest that the applied or realized potentials are the driving forces for their formation irrespective of the deposition technique employed. The technical impact of the present work is that for morphology critical applications it is essential to use potentiostatic deposition to control the morphology whereas for the phase and composition critical applications either deposition technique is suitable provided the desired deposition rates are achieved.

Conclusions

Potentiostatic and galvanostatic deposition techniques were employed to produce nanocrystalline Al–Mg deposits in dendritic form. In the potentiostatic deposits, only featherlike morphology (fcc Al(+Mg) phase containing ~7 atom% Mg) was obtained at E=−4 V and only globular morphology with smooth (fcc Al(+Mg) phase with ~20 atom%Mg) and rough (hcp Mg(+Al) phase with ~80 atom%Mg) formed at E=−5 V. The galvanostatic depositions conducted at apparent current densities of 30 and 60 mA cm^{-2} resulted in both types of morphologies in any deposit. The featherlike dendrites in galvanostatic deposition at 60 mA cm^{-2} eventually showed morphological evolution by forming smooth globular morphology at their tips over which rough globules nucleated. The results of the present study led to the following conclusions:

1. Potentiostatic deposition governs the depositing morphology by providing necessary energy for formation of a single morphology across the whole substrate. In galvanostatic deposition, since no control is exercised over the resulting cathode potential, obtaining uniform morphology throughout the substrate is difficult.
2. The composition and phases of the deposits depend mainly on the applied/realized potentials rather than on the deposition technique. At lower applied/realized potentials, i.e., at E=−4 V or j=30 mA cm^{-2} only fcc Al(+Mg) phase was obtained. At higher applied/ realized potentials of E=−5 V or j=60 mA cm^{-2} hcp Mg(+Al) phase formed over fcc Al(+Mg) phase.
3. The morphological evolution of the featherlike dendrites into smooth globules in galvanostatic deposition was due to high current densities experienced around the tips of the featherlike morphology.

Acknowledgments Support from National Science Foundation (grant number DMR-0605406) is greatly appreciated.

References

1. Maksimovic VM, Pavlovic LJ, Tomic MV (2009) Matalurgija-J Metall 15:19–27
2. Nikolic ND, Popov KI, Pavlovic LJ, Pavlovic MG (2006) Surf Coat Technol 201:560–566
3. Tatiparti SSV, Ebrahimi F (2010) J Electrochem Soc 157:E167–E171
4. Popov KI, Pavlovic MG, Maksimovic MD (1982) J Appl Electrochem 12:525–531
5. Shao S, Zhang G, Zhou H, Sun P, Yuan Z, Li B, Ding D, Chen T (2007) Solid State Sci 9:725–731
6. Markevich E, Levi MD, Aurbach D (2005) J Electroanal Chem 580:231–237
7. Popov KI, Pavjovic MG, Maksimovic MD, Krstajic SS (1978) J Appl Electrochem 8:503–514
8. Tatiparti SSV, Ebrahimi F (2008) J Electrochem Soc 155:D363–D368
9. Tatiparti SSV, Ebrahimi F (2011) Mater Lett 65:1915–1918
10. Tatiparti SSV, Ebrahimi F (2010) J Appl Electrochem 40:2091–2098
11. Jovic VD, Maksimovic V, Pavlovic MG, Popov KI (2006) J Solid State Electrochem 10:373–379
12. Bozzini B, De Gaudenzi GP, Mele C (2004) J Electroanal Chem 563:133–143
13. Scharifker B, Hill G (1983) Electrochim Acta 28:879–889
14. Popov KI, Djokic SS, Grgur BN (2002) Fundamental aspects of electrometallurgy. Kluwer, New York
15. Lee J, Talbot JB (2007) J Electrochem Soc 154:D70–D77
16. Fannin LW, Malpass DB, Sanchez R (1981) USPat: 4299781
17. Simanavicius L, Stakenas A, Sarkis A (1997) Electrochim Acta 42:1581–1586
18. Murray JL (1982) Bull Alloy Phase Diagr 3:60–74
19. Popov KI, Pavlovic MG, Spasojevic MD, Nakic VM (1979) J Appl Electrochem 9:533–536
20. Barton JL, Bockris JOM (1962) Proc R Soc London Ser A 268:485–505
21. Tatiparti SSV, Ebrahimi F (2011) Mater Lett 65:1859–1861